Supporting Information

Hierarchical Core-shell Heterostructure FeMoS@CoFe LDH for Multifunctional Green Applications Boosting Large Current Density Water Splitting

Chun Han[a], Yunhe Zhao[a*], Gong Chen[a], Haiyan Song[a], Xiaoliang Wu[a], Zehua Guo[b], Chunxia Chen[a*]

a. College of Chemistry, Chemical Engineering and Resource Utilization, Northeast Forestry University, 26 Hexing Road, Harbin, 150040, P.R. China.

b. Heilongjiang Provincial Key Laboratory of Nuclear Power System & Equipment, Harbin Engineering University, Harbin 150001, P.R. China.

E-mail addresses: zhaoyunhe@nefu.edu.cn (Y. Zhao), ccx1759@163.com (C. Chen).

1. Experimental section

1.1 Chemicals and materials

Ferric nitrate nonahydrate ($Fe(NO_3)_3 \cdot 9H_2O$, 99%), cobaltous nitrate hexahydrate ($Co(NO_3)_2 \cdot 6H_2O$, 99%), ammonium molybdate ($(NH_4)_6Mo_7O_{24} \cdot 4H_2O$, 99%), ferrous sulfate ($FeSO_4 \cdot 7H_2O$, 99%), thioacetamide (TAA, 99%), and potassium hydroxide (KOH, 85%) were all of analytical grade and used without further purification. The deionized water was used throughout the experiments.

1.2 Synthesis of FeMoS

First, the nickel foam (NF) (about 2×3 cm^2) was cleaned using 1 M HCl aqueous solution, ethanol, and deionized water for 15 minutes respectively. Then, 0.04 M $Fe(NO_3)_3 \cdot 9H_2O$, 0.04 M $(NH_4)_2MoO_4$, and 0.03 M TAA were dissolved in 35 mL deionized water and stirred for 10 min under room temperature. Then the solution was transferred to a 50 ml Teflon-lined steel autoclave with NF and heated at 180 °C for 12 h. The FeMoS precursor was obtained through washing with deionized water and then dried at 60 °C overnight.

1.3 Synthesis of FeMoS@CoFe LDH

The FeMoS@CoFe LDH was prepared via the electrodeposition using a three-electrode configuration with FeMoS, saturated calomel electrode (SCE) and Pt sheet as working electrode, reference electrode and counter electrode, respectively. It was carried out in a mixed solution of 0.015 M $Co(NO_3)_2 \cdot 6H_2O$ and 0.015 M $FeSO_4 \cdot 7H_2O$ by maintaining the potential of -1.0 V (*vs*. SCE) for 100 s, 200 s and 300 s, respectively.

1.4 Synthesis of CoFe LDH

The CoFe LDH nanosheet was direct electrodeposited on NF as working electrode using the same procedure as FeMoS@CoFe LDH.

1.5 Characterizations

The X-ray diffraction (XRD) patterns of the catalysts were recorded on a TD-3500. Scanning electron microscopy (SEM, JSM-7500F) was used to observe the morphologies and structures of the products. Transmission electron microscope (TEM) and corresponding elemental mappings were performed on a JSM-2100 with X-ray energy-dispersive spectroscopy (EDS). The samples were characterized at atomic scale on aberration-corrected high angle annular darkfield scanning transmission electron microscope (AC-HAADF-STEM) of JEM ARM 200F. X-ray photoelectron spectroscopy (XPS) was collected by ESCALAB 250Xi.

1.6 Capillary-fed electrolysis cell connected drainage device

In this device, the polyether sulfone (PES) separator between the electrodes continuously supplies electrolyte to the electrodes through spontaneous capillary action. The electrodes are held against opposite sides of the separator, above the horizontal line of the electrolyte. The bottom end of the separator is dipped in a reservoir, resulting in capillary-induced movement of electrolyte. These electrodes draw liquid from the separator forming a thin electrolyte coating. Applying an appropriate voltage between the electrodes can trigger the electrolysis of water. Due to the ability of the generated H_2 and O_2 to easily penetrate the thin electrolyte layer covering their respective electrodes, the design of the capillary-fed electrolysis cell-drainage device achieves bubble free electrolysis. Gas can be collected directly through exhaust channels and drainage devices.

1.7 Electrochemical analysis

The electrocatalytic performance of the three-electrode system was evaluated on the CHI 660D electrochemical analyzer. The Hg/HgO electrode was used as reference electrode, Pt sheet as the counter electrode in OER, graphite rod as the counter electrode in HER, and as-synthesized samples as the working electrode. The following formula is used for calibrating potential based on reversible hydrogen electrode scale:

$$E_{RHE} = E_{Hg/HgO} + 0.198\ V + 0.059$$

The electrochemical double layer capacitance (C_{dl}) was determined with typical cyclic voltammetry (CV) measurements at various scan rates between 10~50 mV s^{-1}. The calculation formula for C_{dl} is $C_{dl} = (j_a - j_c)/(2 \times v)$, where j_a and j_c are the current densities of the positive and negative electrodes, respectively.

Electrochemically active surface area (ECSA). The ECSA was measured by the C_{dl} method, which was calculated through the following equation:

$$ECSA = \frac{C_{dl}}{C_s} \times S$$

where C_s = 40 mF cm^{-2}, where s represents the physical surface area of the electrode (~ 0.25 cm^2).

Turnover frequency (TOF). TOF was calculated via the following formula according to previous reports.[1, 2]

$$TOF\ per\ site = \frac{\#\ Total\ Hydrogen\ Turn\ Overs/cm^2\ \ geometric\ area}{\#\ Surface\ Sites/cm^2\ geometric\ area}$$

The total number of hydrogen turnovers was calculated from the current density using the following equation:

$$\#_{H_2} = \left(j\frac{mA}{cm^2}\right)\left(\frac{1C\ s^{-1}}{1000\ mA}\right)\left(\frac{1\ mol\ e^-}{96485\ C}\right)\left(\frac{1\ mol\ H_2}{2\ mol\ e^-}\right)\left(\frac{6.022 \times 10^{23} H_2\ molecules}{1\ mol\ H_2}\right)$$

$$= 3.12 \times 10^{15} \frac{H_2/s}{cm^2} per \frac{mA}{cm^2}$$

The total number of effective surface sites was calculated based on the following equation:

$$\frac{\#\ Surface\ sites}{cm^2\ geometric\ area} = \frac{\#\ Surface\ sites\ (flat\ standard)}{cm^2\ geometric\ area} \times Roughness\ factor$$

Here, the roughness factor (RF) was calculated according to the following equation:

$$RF = \frac{C_{dl}(Sample)}{C_{dl}(flat\ standard)}$$

Faraday efficiency (*FE*). The Faraday efficiency of HER/OER was measured using the drainage method. The calculation formula for *FE* is as follows:

$$FE(\%) = \frac{n_{exp}}{n_{theor}} \times 100$$

where n_{exp} and n_{theor} are experimental and theoretical amounts of O_2 or H_2: produced during the OER or HER process, z is the electron transfer number of OER or HER.

According to the Faraday's law, the n_{theor} (O_2) was calculated by the equation:

$$n_{theor} = \frac{I \cdot t}{z \cdot F}(mol)$$

It was determined by a water displacement method and calculated by the ideal gas law:

$$n_{exp} = \frac{p \cdot V}{R \cdot T}(mol)$$

To sum up, the calculation formula for *FE* is as follows:

$$FE(\%) = \frac{n_{exp}}{n_{theor}} \times 100 = \frac{zFV}{ItV_m}$$

where $z = 2$ is the electron transfer number of HER and $z = 4$ is the electron transfer number of OER, F is the Faraday constant (96485 C mol^{-1}), V is the volume of O_2/H_2 produced, I is the current (A), t is the time (s) and V_m is the molar volume of (24.5 L mol^{-1} at 20 °C).

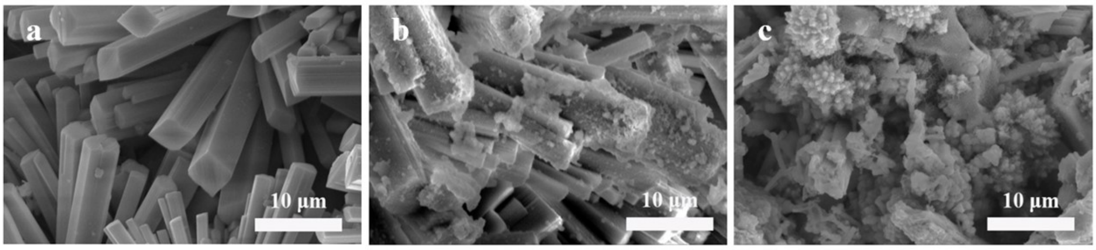

Fig. S1. SEM images of (a) FeMoS. (b) FeMoS@CoFe LDH-100. (c) FeMoS@CoFe LDH-300.

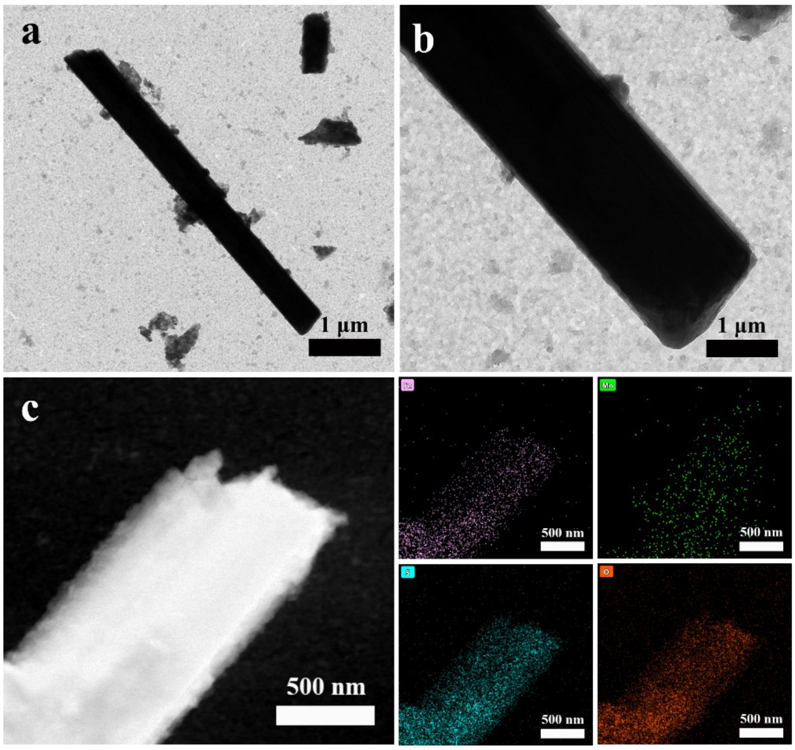

Fig. S2. (a,b) TEM images and (c) Corresponding elemental mapping images of FeMoS.

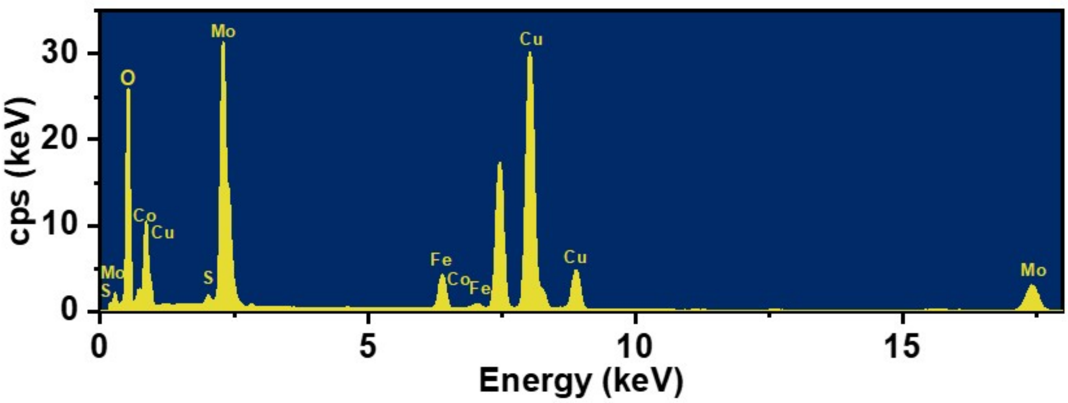

Element	Atomic Fraction (%)	Mass Fraction (%)
Fe	3.43	4.82
Mo	25.76	60.18
Co	0.70	0.98
S	5.81	4.91
O	64.29	29.11

Fig. S3. STEM-EDS spectra of FeMoS@CoFe LDH.

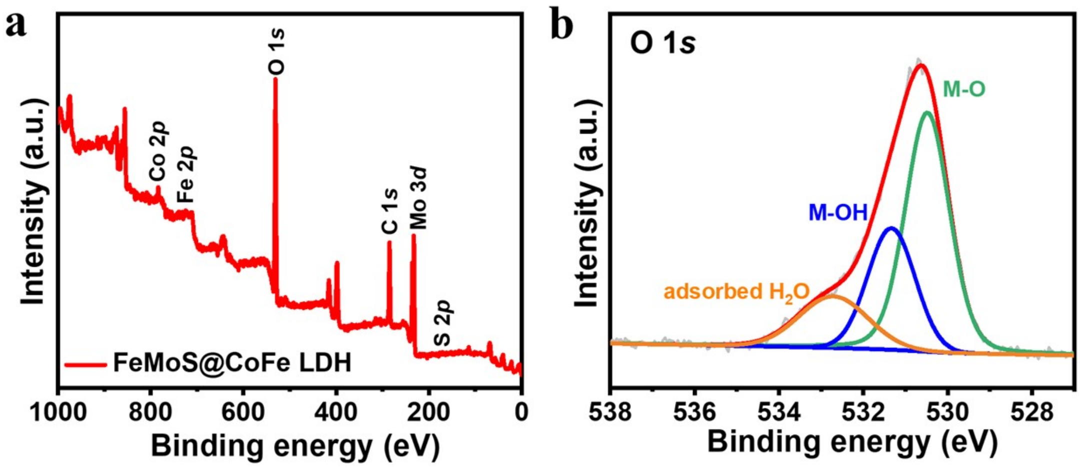

Fig. S4. (a) XPS survey spectrum of FeMoS@CoFe LDH. (b) The high-resolution spectra of O 1*s*.

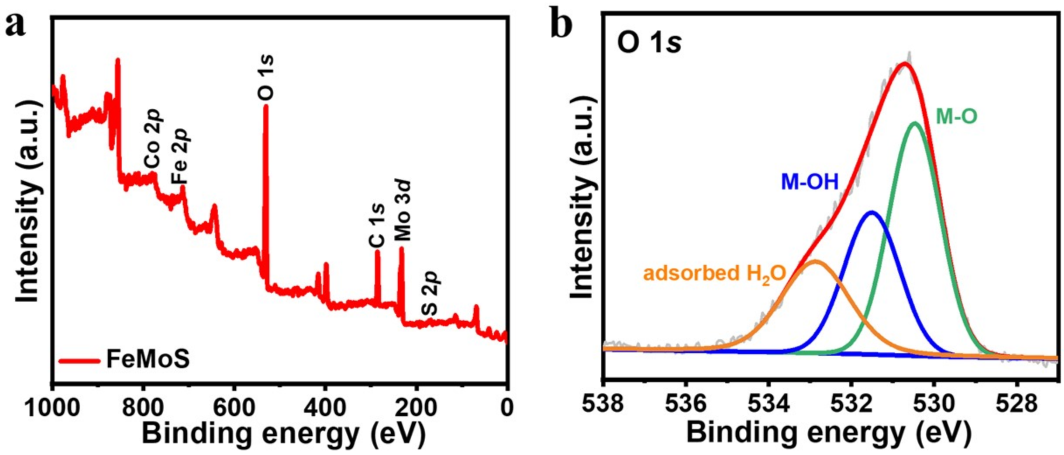

Fig. S5. (a) XPS survey spectrum of FeMoS. (b) The high-resolution spectra of O 1*s*.

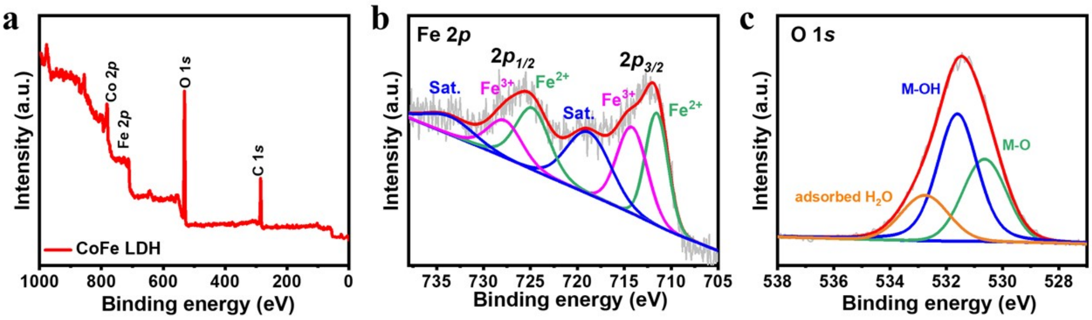

Fig. S6. (a) XPS survey spectrum of CoFe LDH. The high-resolution spectra of (b) Fe 2*p*. (c) O 1*s*.

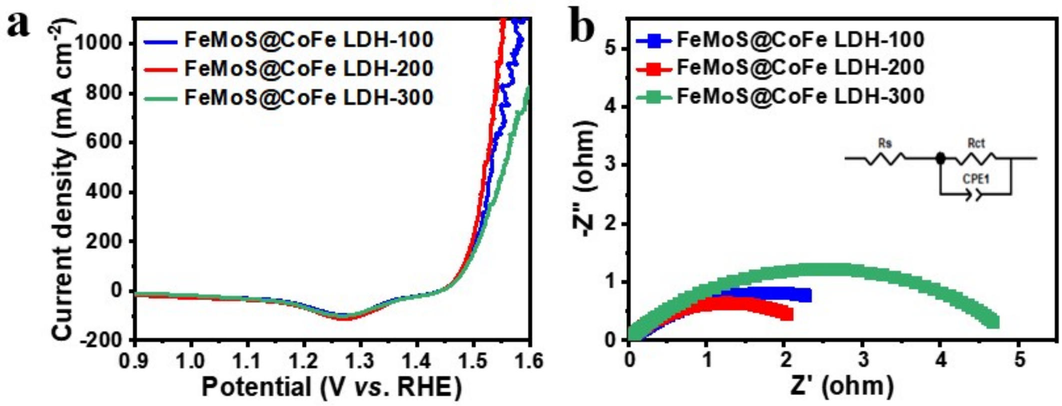

Fig. S7. OER performances of (a) LSV curves. (b) Nyquist plots and equivalent circuits of FeMoS@CoFe LDH-100, FeMoS@CoFe LDH -200 and FeMoS@CoFe LDH-300.

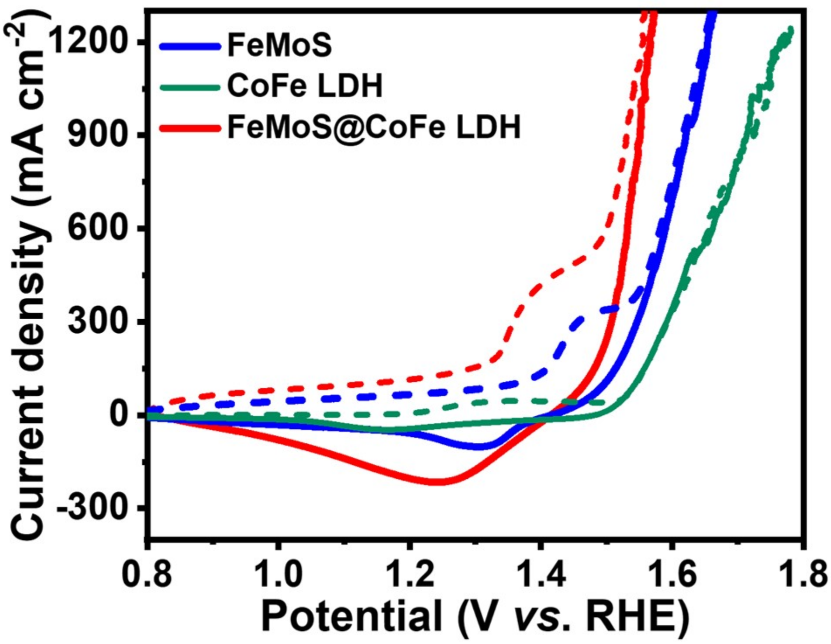

Fig. S8. Forward and backward voltammogram in OER.

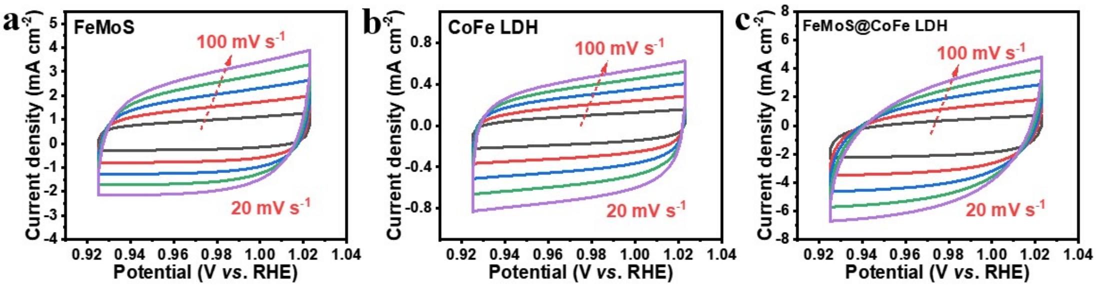

Fig. S9. CV curves of (a) FeMoS. (b) CoFe LDH and (c) FeMoS@CoFe LDH at various scan rates (20, 40, 60, 80 and 100 mV s^{-1}) in the non-Faradic region (0.923 - 1.023 V *vs*. RHE) during OER process.

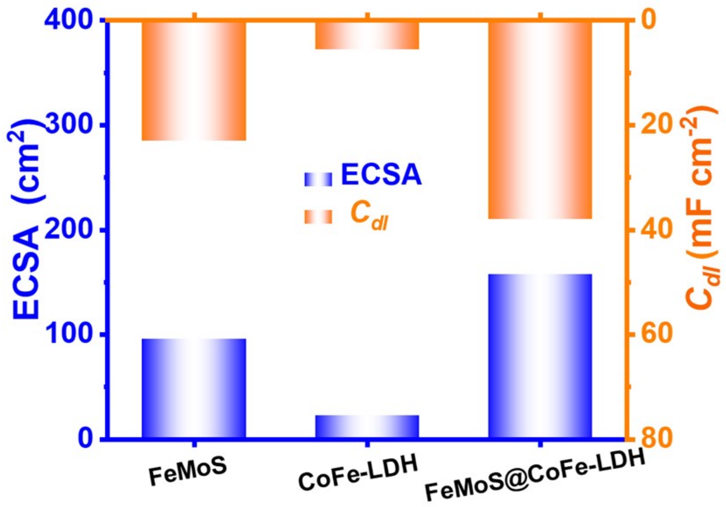

Fig. S10. Double Y-axis bar chart of ECSA and C_{dl} during OER process.

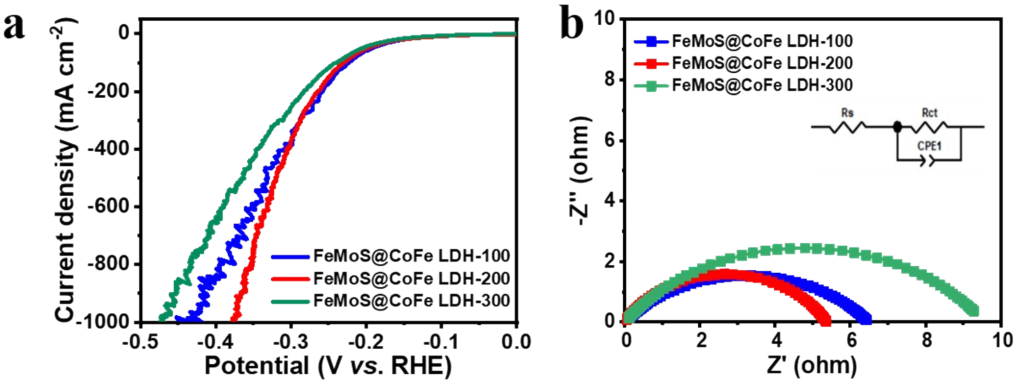

Fig. S11. HER performances of (a) LSV curves. (b) Nyquist plots and equivalent circuits of FeMoS@CoFe LDH-100, FeMoS@CoFe LDH -200 and FeMoS@CoFe LDH-300.

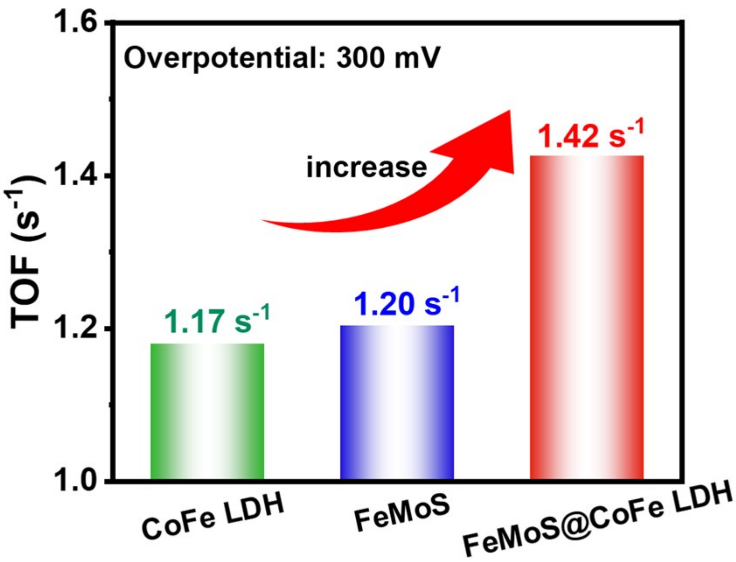

Fig. S12. TOF values at the overpotential of 300 mV in HER.

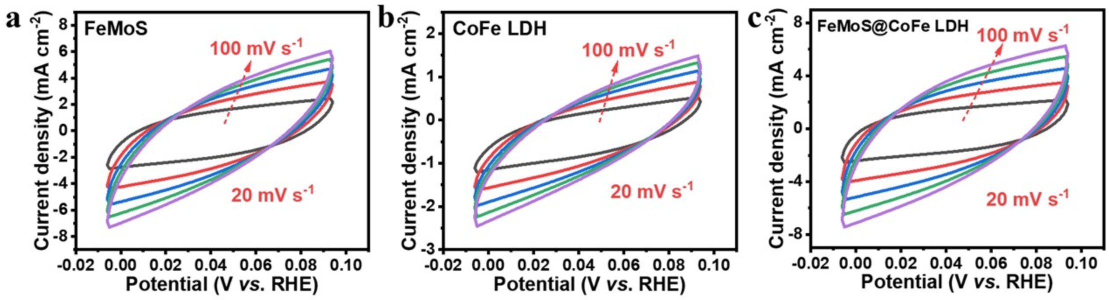

Fig. S13. CV curves of (a) FeMoS. (b) CoFe LDH and (c) FeMoS@CoFe LDH at various scan rates (20, 40, 60, 80 and 100 mV s^{-1}) in the non-Faradic region (-0.006-0.094 V *vs*. RHE) during HER process.

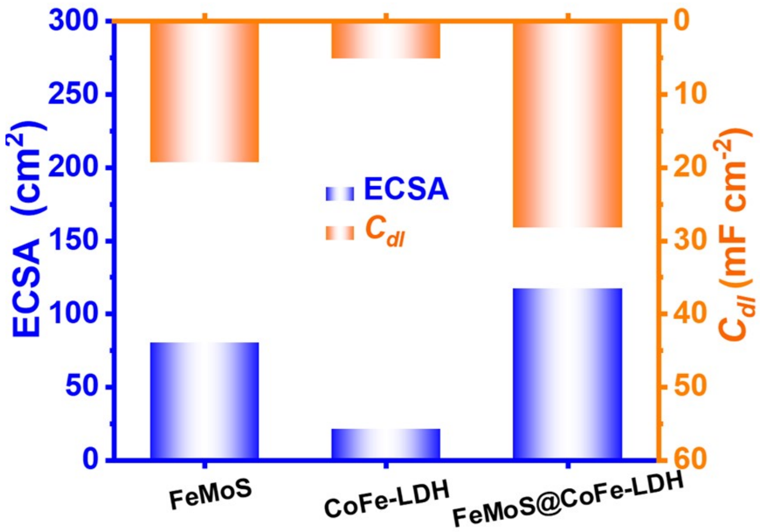

Fig. S14. Double Y-axis bar chart of ECSA and C_{dl} during HER process.

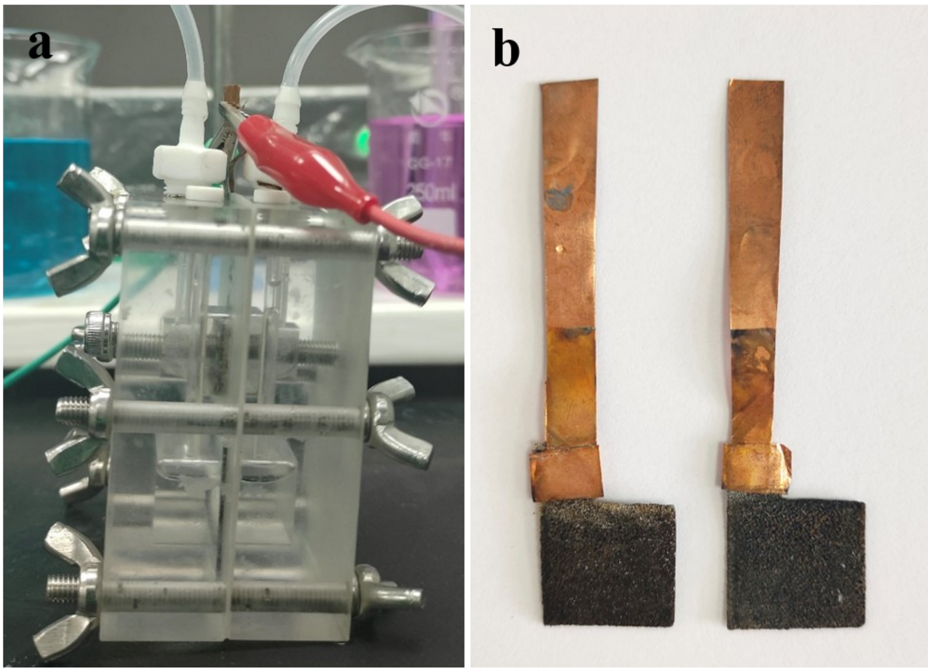

Fig. S15. Optical photos of (a) Capillary-fed electrolysis cell. (b) Cathode and anode.

Table S1. Comparison of OER activity data for various catalysts.

Catalysts	Current density (mA cm^{-2})	Overpotential (mV)	Tafel (mV dec^{-1})	Ref.
Co_9S_8@Fe_3O_4	500	350	54	[3]
IrNi-$FeNi_3$/NF	500	300	36.01	[4]
(Ni-MoO_2)@C/NF	1000	365	62	[5]
NiCo@C-NiCoMoO/NF	1000	390	75.15	[6]
Ni/MoO_2@CN	1000	420	48	[7]
Sn-$Ni(OH)_2$	1000	460	62	[8]
Ni_2P-Fe_2P/NF	1000	337	86	[9]
NiFe LDH/NiS	1000	325	60.1	[10]
Ni/Fe_3O_4	1000	338	44	[11]
FeMoS@CoFe LDH	**500**	**290**	**48.0**	**This work**
FeMoS@CoFe LDH	**1000**	**320**		

Table S2. Comparison of HER activity data for various catalysts.

Catalysts	Current density (mA cm^{-2})	Overpotential (mV)	Ref.
Ni-ZIF/Ni-B@NF	100	282	[12]
FeMn-MOF/NF	100	382	[13]
Pt/C	500	347	[14]
A-NiCo LDH/NF	1000	381	[15]
HC-MoS_2/Mo_2C	1000	441	[16]
Sn-$Ni(OH)_2$	1000	556	[8]
Ni/Fe_3O_4	1000	387	[11]
Sn-Ni_3S_2/NF	1000	570	[17]
FeMoS@CoFe LDH	**100**	**229**	**This work**
FeMoS@CoFe LDH	**500**	**319**	**This work**
FeMoS@CoFe LDH	**1000**	**376**	**This work**

Table S3. Comparison of water splitting performance of FeMoS@CoFe LDH with other electrocatalysts at the current density of 500 mA cm^{-2} in 1 M KOH.

Catalysts	Voltage (V)	Ref.
$MoNi_4$/SSW || SSW Rs-12h	1.978	[18]
$CoMoS_x$/NF || $CoMoS_x$/NF	1.89	[19]
Co_4N-CeO_2 || $CoMoS_x$/NF	1.99	[20]
Pt/C || IrO_2	2.01	[19]
(Ni-Fe)S_x/NiFe$(OH)_y$/NF || (Ni-Fe)S_x/NiFe$(OH)_y$/NF	2.12	[21]
$Co_{0.8}Ru_{0.2}O_x$@NC || $Co_{0.8}Ru_{0.2}O_x$@NC	1.86	[22]
(Fe, Ni)$_2$P@Ni_2P || (Fe, Ni)$_2$P@Ni_2P	1.838	[23]
NiCo(nf)-P || NiCo(nf)-P	1.86	[24]
NiCoP/NF || NiCoP/NF	1.83	[25]
NF-CH-O || NF-CH-O	1.877	[26]
FeMoS@CoFe LDH || FeMoS@CoFe LDH	**1.79**	**This work**

Video S1. The combination of capillary-fed electrolysis cell and drainage device.

Video S2. Solar-to-water electrolysis system.

Video S3. Wind-to-water electrolysis system.

References

1. L. Yu, I. K. Mishra, Y. Xie, H. Zhou, J. Sun, J. Zhou, Y. Ni, D. Luo, F. Yu, Y. Yu, S. Chen and Z. Ren, *Nano Energy*, 2018, **53**, 492-500.
2. L. Yu, L. Wu, S. Song, B. McElhenny, F. Zhang, S. Chen and Z. Ren, *ACS Energy Lett*, 2020, **5**, (8), 2681-2689.
3. Q. Ji, Y. Kong, H. Tan, H. Duan, N. Li, B. Tang, Y. Wang, S. Feng, L. Lv and C. Wang, *ACS Catal*, 2022, **12**, (8), 4318-4326.
4. Y. Wang, G. Qian, Q. Xu, H. Zhang, F. Shen, L. Luo and S. Yin, *Appl Catal B*, 2021, **286**, 119881.
5. G. Qian, J. Chen, L. Luo, T. Yu, Y. Wang, W. Jiang, Q. Xu, S. Feng and S. Yin, *ACS Sustainable Chem Eng*, 2020, **8**, (32), 12063-12071.
6. G. Qian, J. Chen, T. Yu, L. Luo and S. Yin, *Nano-Micro Lett*, 2021, **13**, (1), 77.
7. G. Qian, J. Chen, T. Yu, J. Liu, L. Luo and S. Yin, *Nano-Micro Lett*, 2022, **14**, 1-15.
8. J. Jian, X. Kou, H. Wang, L. Chang, L. Zhang, S. Gao, Y. Xu and H. Yuan, *ACS Appl Mater Interfaces*, 2021, **13**, (36), 42861-42869.
9. L. Wu, L. Yu, F. Zhang, B. McElhenny, D. Luo, A. Karim, S. Chen and Z. Ren, *Adv Funct Mater*, 2021, **31**, (1), 2006484.
10. Q. Wen, K. Yang, D. Huang, G. Cheng, X. Ai, Y. Liu, J. Fang, H. Li, L. Yu and T. Zhai, *Adv Energy Mater*, 2021, **11**, (46), 2102353.
11. W. Xu, W. Zhong, C. Yang, R. Zhao, J. Wu, X. Li and N. Yang, *J Energy Chem*, 2022, **73**, 330-338.
12. H. Xu, B. Fei, G. Cai, Y. Ha, J. Liu, H. Jia, J. Zhang, M. Liu and R. Wu, *Adv Energy Mater*, 2020, **10**, (3), 1902714.
13. H. Guan, N. Wang, X. Feng, S. Bian, W. Li and Y. Chen, *Colloids Surf A*, 2021, **624**, 126596.
14. C. Yang, W. Zhong, K. Shen, Q. Zhang, R. Zhao, H. Xiang, J. Wu, X. Li and N. Yang, *Adv Energy Mater*, 2022, **12**, (16), 2200077.
15. H. Yang, Z. Chen, P. Guo, B. Fei and R. Wu, *Appl Catal B*, 2020, **261**, 118240.
16. C. Zhang, Y. Luo, J. Tan, Q. Yu, F. Yang, Z. Zhang, L. Yang, H. Cheng and B. Liu, *Nat*

Commun, 2020, **11**, (1), 3724.

17. J. Jian, L. Yuan, H. Qi, X. Sun, L. Zhang, H. Li, H. Yuan and S. Feng, *ACS Appl Mater Interfaces*, 2018, **10**, (47), 40568-40576.
18. V. R. Jothi, K. Karuppasamy, T. Maiyalagan, H. Rajan, C. Jung and S. C. Yi, *Adv Energy Mater*, 2020, **10**, (24), 1904020.
19. X. Shan, J. Liu, H. Mu, Y. Xiao, B. Mei, W. Liu, G. Lin, Z. Jiang, L. Wen and L. Jiang, *Angew Chem Int Ed*, 2020, **59**, (4), 1659-1665.
20. H. Sun, C. Tian, G. Fan, J. Qi, Z. Liu, Z. Yan, F. Cheng, J. Chen, C. P. Li and M. Du, *Adv Funct Mater*, 2020, **30**, (32), 1910596.
21. Q. Che, Q. Li, Y. Tan, X. Chen, X. Xu and Y. Chen, *Appl Catal B*, 2019, **246**, 337-348.
22. Q. Yang, Y. Cui, Q. Li, J. Cai, D. Wang and L. Feng, *ACS Sustainable Chem Eng*, 2020, **8**, (32), 12089-12099.
23. Y. Li, X. Yu, J. Gao and Y. Ma, *Chem Eng J*, 2023, **470**, 144373.
24. Z. Xu, C. Yeh, J. Chen, J. T. Lin, K. Ho and R. Y. Lin, *ACS Sustainable Chem Eng*, 2022, **10**, (35), 11577-11586.
25. H. Hu, Y. Li, Y. Shao, K. Li, G. Deng, C. Wang and Y. Feng, *J Power Sources*, 2021, **484**, 229269.
26. Y. Qiu, Z. Liu, X. Zhang, A. Sun and J. Liu, *J Colloid Interface Sci*, 2022, **625**, 50-58.